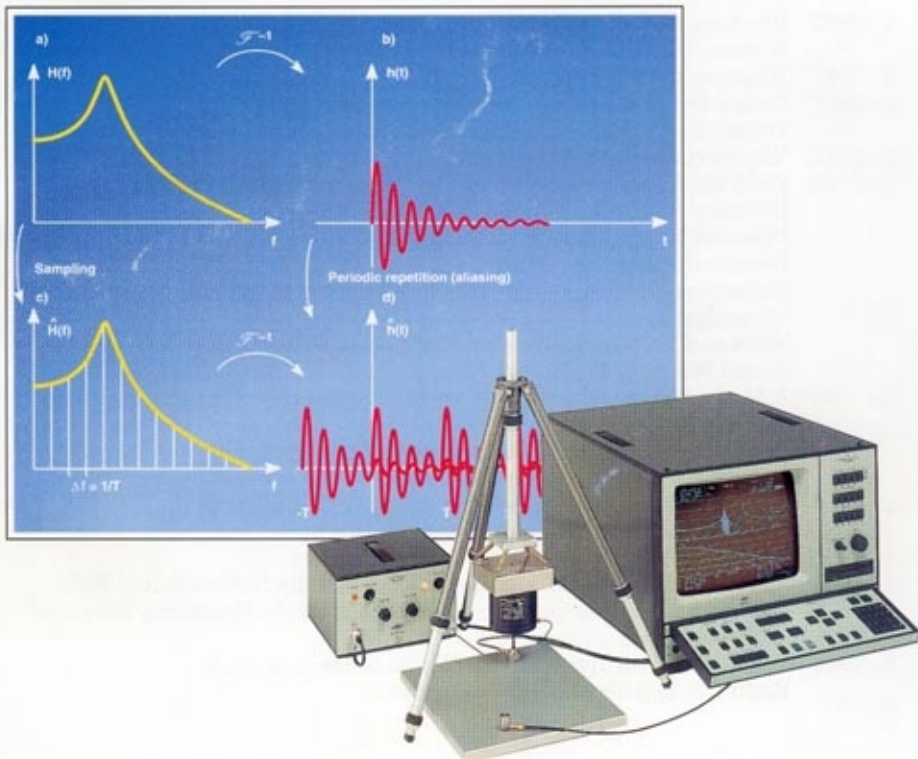


Technical Review

No. 2 – 1994

Damping Measurements – From Impulse Response Functions
– From Resonance and Non-resonance Excitation Techniques



Brüel & Kjær 

Previously issued numbers of Brüel & Kjær Technical Review

- 1 –1994 Digital Filter Techniques vs. FFT Techniques for Damping Measurements (Damping Part I)
- 2-1990 Optical Filters and their Use with the Type 1302 & Type 1306 Photoacoustic Gas Monitors
- 1 –1990 The Brüel & Kjær Photoacoustic Transducer System and its Physical Properties
- 2-1989 STSF — Practical instrumentation and application
Digital Filter Analysis: Real-time and Non Real-time Performance
- 1 –1989 STSF — A Unique Technique for scan based Near-Field Acoustic Holography without restrictions on coherence
- 2-1988 Quantifying Draught Risk
- 1 –1988 Using Experimental Modal Analysis to Simulate Structural Dynamic Modifications
Use of Operational Deflection Shapes for Noise Control of Discrete Tones
- 4-1987 Windows to FFT Analysis (Part II)
Acoustic Calibrator for Intensity Measurement Systems
- 3-1987 Windows to FFT Analysis (Part I)
- 2 –1987 Recent Developments in Accelerometer Design
Trends in Accelerometer Calibration
- 1 –1987 Vibration Monitoring of Machines
- 4-1986 Field Measurements of Sound Insulation with a Battery-Operated Intensity Analyzer
Pressure Microphones for Intensity Measurements with Significantly Improved Phase Properties
Measurement of Acoustical Distance between Intensity Probe Microphones
Wind and Turbulence Noise of Turbulence Screen, Nose Cone and Sound Intensity Probe with Wind Screen
- 3 –1986 A Method of Determining the Modal Frequencies of Structures with Coupled Modes
Improvement to Monoreference Modal Data by Adding an Oblique Degree of Freedom for the Reference
- 2 –1986 Quality in Spectral Match of Photometric Transducers
Guide to Lighting of Urban Areas
- 1 –1986 Environmental Noise Measurements
- 4 –1985 Validity of Intensity Measurements in Partially Diffuse Sound Field
Influence of Tripods and Microphone Clips on the Frequency Response of Microphones
- 3 –1985 The Modulation Transfer Function in Room Acoustics
RASTI: A Tool for Evaluating Auditoria

(Continued on cover page 3)

Technical Review

No.2 -1994

Contents

Damping Part II

The use of Impulse Response Function for Modal Parameter Estimation.. 1

by *Svend Gade & Henrik Herlufsen*

Complex Modulus and Damping Measurements using Resonant and
Non-resonant Methods 28

by *S. Gade, K. Zaveri, H. Konstantin-Hansen and H. Herlufsen*

Copyright © 1994, Brüel & Kjær A/S

All rights reserved. No part of this publication may be reproduced or distributed in any form, or
by any means, without prior written permission of the publishers. For details, contact:
Brüel & Kjær A/S, DK-2850 Nærum, Denmark.

Editor: K. Zaveri Photographer: Peder Dalmo
Layout: Judith Sarup Printed by Nærum Offset

The use of Impulse Response Function for Modal Parameter Estimation

by *Svend Gade & Henrik Herlufsen*

Abstract

This article discusses the errors that are introduced when calculating the impulse response function from the frequency response function using DFT/FFT analysis technique.

The impulse response function is used in many applications of system analysis where a description of the system characteristics is preferred in the time domain rather than in the frequency domain. The case where the system is a single degree of freedom system (SDOF), with viscous damping, is analysed. It is shown that the estimated impulse response function is not described by a single exponentially decaying sine wave but rather as a sum of exponentially decaying sine waves. It is important to apply this slightly more complex model when the measurements are to be used for mathematical modelling of systems containing lightly damped resonances and where measurements free of the influence of leakage are performed.

This article represents an expansion of papers presented at the Modal Analysis Conference ISMA 15, held in Leuven, Belgium 1990 and included in the Proceedings of IMAC 9, Firenze, Italy 1991.

Resume

Cet article décrit les erreurs pouvant survenir lors du calcul de la réponse impulsionale à partir de la fonction de réponse en fréquence, dans le cadre d'une analyse DFT/FFT.

La fonction de réponse impulsionale intervient lorsque, pour décrire les caractéristiques d'un système, les techniques d'analyse en fréquence dans le domaine temporel sont préférées à celles du domaine fréquentiel. Le cas d'un système à un degré de liberté (SDOF) avec amortisseurs à fluide est ici exa-

miné. Il est montré que la fonction de réponse impulsioimelle estimée n'est pas représentée par une seule onde sinusoïdale à décroissement exponentiel mais plutôt par une somme de ces ondes. Il est important d'appliquer ce modèle un peu plus complexe lorsque les mesures doivent servir de base à des modèles mathématiques de systèmes présentant des résonances légèrement amorties, et dans le cas de mesures où l'influence de fuites n'est pas prise en compte.

Cet article se place dans le prolongement des articles exposés lors de la conférence sur l'analyse modale ISMA 15, à Louvain en 1990 et inclus dans le compte rendu de la conférence IMAC qui s'est tenue à Florence en 1991.

Zusammenfassung

In diesem Artikel werden die Fehler diskutiert, die entstehen, wenn die Impulsantwortfunktion mit DFT/FFT-Analysetechnik aus der Frequenzgangfunktion berechnet wird.

Die Impulsantwortfunktion wird bei zahlreichen Systemanalyse-Applikationen verwendet, wenn für die Beschreibung der Systemcharakteristiken der Zeitbereich gegenüber dem Frequenzbereich bevorzugt wird. Es wird der Fall eines Systems mit einem einzigen Freiheitsgrad (SDOF) und viskoser Dämpfung untersucht. Es wird gezeigt, daß die geschätzte Impulsantwortfunktion nicht durch eine einzelne exponentiell abklingende Sinuswelle, sondern eher als die Summe exponentiell abklingender Sinuswellen beschrieben wird. Es ist wichtig, dieses etwas komplexere Modell für Messungen anzuwenden, die zur mathematischen Modellierung von Systemen mit leicht gedämpften Resonanzen dienen, sowie für Messungen, die unbeeinflußt von Leckagen durchgeführt werden.

Der Artikel stellt eine Erweiterung der Dokumentation dar, die auf der Modalanalyse-Konferenz ISMA 15 in Leuven, Belgien, 1990 präsentiert und auf der IMAC 9, Florenz, Italien, 1991 in die Berichterstattung aufgenommen wurde.

Nomenclature

dB	decibels, ten times the logarithm to a (power) ratio
e	base of natural logarithm, 2.72
i	an integer ($-\infty < i \leq 0$ or $0 \leq i < \infty$)
j	imaginary number, $\sqrt{-1}$
k	spectrum line number (an integer)
m	milli. 10^{-3}

n	relative time constant
s	seconds
A_0	constant amplitude, Residue
C, C1, C2	amplitude (bias) error
B & K	Brüel & Kjær
DFT	Discrete Fourier Transform
FFT	Fast Fourier Transform, fast version of DFT
FRF	Frequency response function
$H(j)$	Frequency response function
Hz	Hertz [s^{-1}]
IDFT	Inverse Discrete Fourier Transform
IRF	Impulse response function
$h(t)$	Impulse response function
L ϵ	amplitude error in dB
MDOF	Multi Degree of Freedom
R	residue
$\angle R$	angle of residue
SDOF	Single Degree of Freedom
SMS	Structural Measurement System, Inc.
STAS	Structural Testing and Analysis System
T	FFT record length
$\hat{\cdot}$	estimated value
ϵ_b	amplitude (bias) error
ζ	fraction of critical damping, damping ratio
ϕ	phase error [Radians]
σ	decay constant [s^{-1}]
σ_m	measured decay constant [s^{-1}]
σ_w	decay constant for exponential weighting [s^{-1}]
t	time [s]
τ	time constant [s]
ω_d	damped natural frequency [Rad/s]
Δf_{3dB}	3 dB bandwidth [Hz]
Δf	FFT line spacing [Hz]
%	per cent, 10^{-2}
F	Fourier Transform
F^{-1}	Inverse Fourier Transform

Introduction

When measuring system characteristics, an input and an output must be defined. This will be in terms of a certain physical parameter, point, position, direction, etc. Simultaneous measurement of the input signal to the system (the excitation) and the output signal from the system (the response) allows calculation of the system characteristics such as damping. The function describing the dynamic behaviour of the system in the time domain is the impulse response function $h(t)$. The corresponding frequency domain function is the frequency response function $H(f)$.

Fig. 1 shows a system with input signal $a(t)$ and output signal $b(t)$. The Fourier spectra of $a(t)$ and $b(t)$ are $A(f)$ and $B(f)$ respectively, F denotes the Fourier Transform.

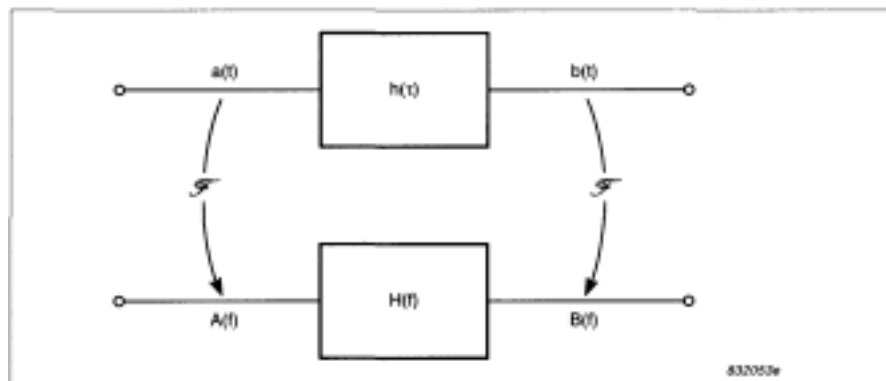


Fig. 1. System with input signal $a(t)$ and output signal $b(t)$. The Fourier Transforms of $a(t)$ and $b(t)$ are $A(f)$ and $B(f)$ respectively

For this description to be valid the system is assumed to be linear. This means that if $a_1(t)$ and $a_2(t)$ produce the outputs $b_1(t)$ and $b_2(t)$ respectively, then the input $a_1(t) + a_2(t)$ must produce the output $b_1(t) + b_2(t)$.

Physically the impulse response function $h(t)$ is the response of the system to a unit impulse signal $\delta(t)$. $\delta(t)$, also called a Dirac delta function, is an infinitely short and infinitely high impulse at $t = 0$. Its time integral is unity and its Fourier spectrum is unity at all frequencies, i.e.

$$\int_{-\infty}^{\infty} \delta(t) dt = 1 \quad (1)$$

and

$$\mathcal{F}\{\delta(t)\} = 1 \quad -\infty < f < \infty \quad (2)$$

In order to find the relationship between the input signal and the output signal we can consider any input signal $a(t)$ as a superposition of weighted and time-shifted delta functions, i.e.

$$a(t) = \int_{-\infty}^{\infty} a(t') \delta(t-t') dt' \quad (3)$$

Each of these weighted and time-shifted delta functions $a(t') \delta(t-t')$ at the input will produce a corresponding weighted and time-shifted impulse response $a(t') h(t-t')$ at the output. The output signal $b(t)$ caused by the input signal $a(t)$ will therefore be the superposition of these individual contributions and

$$b(t) = \int_{-\infty}^{\infty} a(t') h(t-t') dt' = a(t) * h(t) \quad (4)$$

where $*$ denotes convolution.

The frequency response function $H(f)$ is defined as the complex ratio of $B(f)$ and $A(f)$, i.e.

$$H(f) = \frac{B(f)}{A(f)} \quad (5)$$

or

$$B(f) = H(f) A(f) \quad (6)$$

$h(t)$ and $H(f)$ are related via the Fourier transform and therefore contain the same information about the dynamic behaviour of the system.

$$H(f) = \mathcal{F}\{h(t)\} \quad (7)$$

Since the multiplication involved in eq.(6) in most cases is a much simpler operation than the convolution in eq.(4), description and interpretation of phenomena is often done in the frequency domain.

In some applications, however, it is advantageous to present the information in the time (or delay) domain rather than in the frequency domain. Examples of such applications are:

- Determination of time delays in systems
- Identification of transmission paths
- Measurements of decays and determination of damping values
- Mathematical modelling and curvefitting for extraction of system parameters

In this article we will be dealing with the last two application examples. They represent situations where the impulse response function is prone to a bias error when calculated via an inverse Fourier transform from a leakage free measurement of the frequency response function using DFT/FFT technique.

When the system under investigation contains lightly damped resonances, the estimated impulse response function will be biased in both amplitude and phase.

Lightly damped resonances in a system causes the impulse response function to be long with decaying oscillations, which in the frequency domain corresponds to sharp, narrow peaks in the frequency response function.

If the record length in the FFT analysis is not sufficiently long compared to the time constant of the decay in the impulse response function, the bias error is observed. In the frequency domain this means that the above-mentioned bias error is observed if the resonance peak in the frequency response function is narrower than the resolution in the analysis even though the calculated samples of the frequency response function are free of the influence of leakage.

Using the impulse response function for system parameter identification (curvefitting) and modelling, such as in modal analysis, the bias error will be reflected in the residues for the resonances and thereby in the estimated mode shapes for the structure, while the natural frequency and damping will be correctly estimated.

Theory

Let us look at a simple single degree of freedom (SDOF) system. Fig. 2 shows a mechanical SDOF system with viscous damping. It consists of a mass m supported by a spring with a spring constant k and a viscous damper with damping coefficient c .

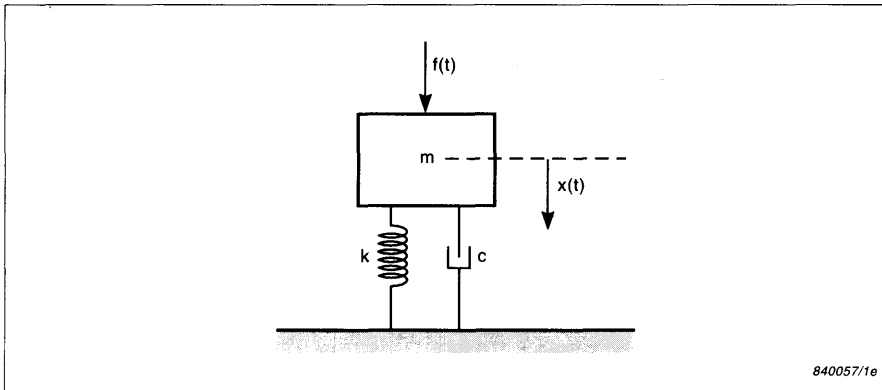


Fig. 2. Mechanical single degree of freedom system

The input is denoted to be the force $f(t)$ acting on the mass and the output is the displacement $x(t)$ of the mass.

The frequency response function (FRF), in this case called the compliance of the system, is given by

$$H(f) = \frac{X(f)}{F(f)} = \frac{1/m}{-\omega^2 + j\omega \frac{c}{m} + \frac{k}{m}} = \frac{R}{j\omega - (j\omega_d - \sigma)} + \frac{R^*}{j\omega - (-j\omega_d - \sigma)} \quad (8)$$

where ω_d , the damped natural frequency, is given by

$$\omega_d = \sqrt{\frac{k}{m} - \frac{c^2}{4m^2}} \quad (9)$$

and σ , the decay constant, is given by

$$\sigma = \frac{c}{2m} \quad (10)$$

and R is a scaling constant, called the residue. (In the literature the residue is sometimes scaled differently by a factor of 2 and/or a 90 degree phase shift).

An example of the magnitude of $H(f)$ is shown in Fig.3a). The corresponding impulse response function (IRF) is an exponentially decaying sine wave as shown in Fig. 3b).

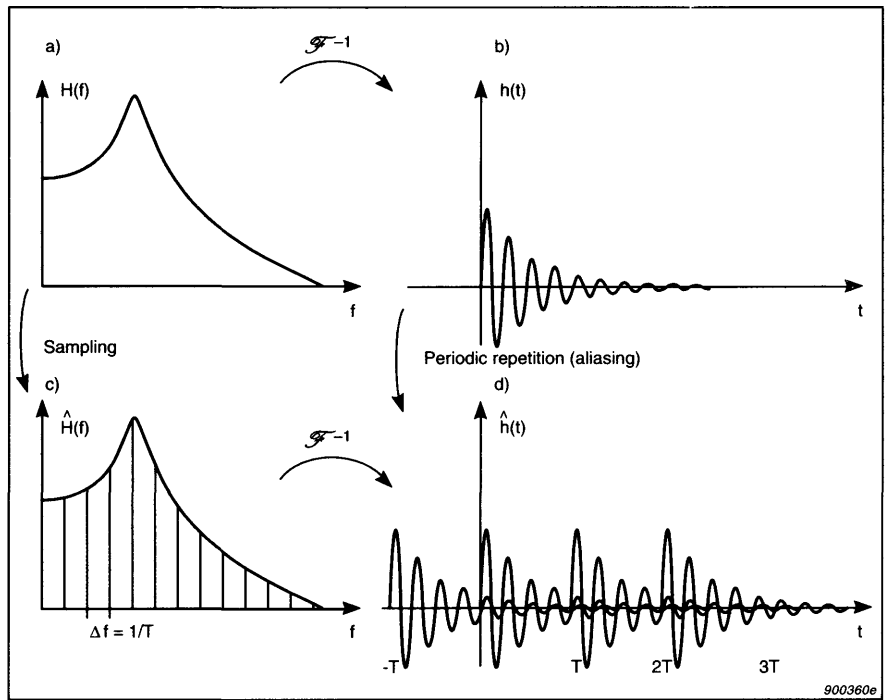


Fig. 3. a) Frequency Response Function (FRF) of a Single Degree of Freedom (SDOF) model, b) Impulse Response Function (IRF) of a SDOF model, c) Sampled FRF of a SDOF model, d) IRF of a sampled FRF SDOF model

Mathematically the IRF is given by

$$h(t) = A_o e^{-\sigma t} \sin(\omega_d t) \quad 0 \leq t \quad (11)$$

$h(t)$ is thus a product of the three terms. $A_o = j2R$ is a (complex) scaling factor given by the residue R , except for a factor of 2 and a 90 degree phase shift. $e^{-\sigma t}$ is the exponentially decaying term, determined by the viscous damping and called the damping term. $\sin(\omega_d t)$ is the term that oscillates at a frequency which is the damped natural frequency.

If a leakage free measurement of the FRF is performed, the calculated lines in the estimated FRF are samples of the continuous ("true") FRF. The "sampling rate" is the line spacing Δf , given by the frequency span divided by the number of spectral lines in the FFT analysis. This is shown in Fig.3c).

Leakage free measurements can be obtained by using a periodic input signal (excitation waveform) with a period equal to the record length in the analysis. Pseudo-random, multisine and periodic random are examples of such excitation signals. See [1] for a discussion of this.

Another possibility is to apply a burst random signal whose burst length is sufficiently short to keep both the excitation as well as the response signals shorter than the record length.

Rectangular weighting should be used in the FFT analysis in all these cases.

Sampling in one domain corresponds to periodic repetition in the other domain, since multiplication by a periodic delta function (here with period $\Delta f = 1/T$) in one domain corresponds to a convolution with a periodic delta function (here with period $T = 1/\Delta f$) in the other domain.

This means that the IRF is repeated every T seconds, where $T = 1/\Delta f$ is the record length in the FFT as shown in Fig. 3d). The estimated IRF is thus given by

$$\hat{h}(t) = \sum_{i=-\infty}^{0} A_o e^{-\sigma(t-iT)} \sin(\omega_d(t-iT)) \quad 0 \leq t < T \quad (12)$$

where i is an integer. The estimated IRF, $\hat{h}(t)$ is said to be aliased, since $h(t)$ is longer than the record length, T causing an interference by the periodic repetition.

Eq. (12) can also be written as

$$\begin{aligned}
\hat{h}(t) &= A_o e^{-\sigma t} \sum_{i=-\infty}^0 e^{i\sigma T} \sin(\omega_d(t-iT)) \quad 0 \leq t < T \\
&= A_o e^{-\sigma t} \sum_{i=-\infty}^0 e^{iT/\tau} \sin(\omega_d t - i\omega_d/\Delta f) \quad 0 \leq t < T
\end{aligned} \tag{13}$$

which, in comparison with eq.(11), shows that the decay rate (i.e. the estimated damping) and the natural frequency are unaffected by the aliasing, while the magnitude and the phase of the IRF are dependent on record length, T , relative to time constant, τ ($= 1/\sigma$), and on the location of damped natural frequency, ω_d , relative to the location of the frequency lines. As a simple interpretation we can conclude the following:

If ω_d coincides with a frequency line, all the decaying sine waves will be in phase and have an additive or constructive effect. If ω_d lies exactly between two lines, every second decaying sine wave will be in phase, while the rest will be in opposite phase giving a subtractive or destructive effect. In the first case the residue will be overestimated, while in the second case the residue will be underestimated.

In these two cases there is no phase error, while in the more general case, a phase error is also observed.

Case 1: Resonance Coinciding with a DFT Frequency Line

In the general case and only for $0 \leq t < T$ and using complex notation, equation (13) becomes

$$\hat{h}(t) = A_o e^{-\sigma t} \frac{1}{2j} \sum_{i=-\infty}^0 e^{i\sigma T} \cdot e^{j\omega_d t} (e^{-j\omega_d iT} - e^{-j\omega_d t} \cdot e^{j\omega_d iT}) \tag{14}$$

For a resonance coinciding with spectrum line number k we have

$$\omega_d = 2\pi k \Delta f \quad (\text{and } T = 1/\Delta f) \tag{15}$$

Thus we have

$$\omega_d i T = 2\pi \cdot i \cdot k \quad (16)$$

which is a multiple of 2π .

Equation (14) can now be written as

$$\begin{aligned} \hat{h}(t) &= A_o e^{-\sigma t} \sum_{i=-\infty}^0 e^{i\sigma T} \left(\frac{e^{j\omega_d t} - e^{-j\omega_d t}}{2j} \right) \\ &= A_o e^{-\sigma t} \sin(\omega_d t) \sum_{i=-\infty}^0 e^{i\sigma T} \end{aligned} \quad (17)$$

Comparing eq. (17) with eq. (11) it is seen that the (amplitude) error, ε_b , for the exponentially decaying sine wave can be written as:

$$\varepsilon_b = \sum_{i=-\infty}^0 e^{i\sigma T} = \sum_{i=0}^{\infty} e^{-i\sigma T} = \frac{1}{1-e^{-T\sigma}} = \frac{1}{1-e^{-T/\tau}} \quad (18)$$

As a first order approximation we have

$$\varepsilon_b \approx \frac{\tau}{T} \quad (\text{for } \tau > 3 \cdot T) \quad (19)$$

Equation (19) shows that the amplitude error is proportional to the time constant of the system if the time constant is considerably longer than the DFT/FFT record length, and that the amplitude is overestimated.

On a dB (logarithmic) scale the error can be expressed as:

$$L_e = -20 \log(1 - e^{-\sigma T}) \quad \text{dB} \quad (20)$$

and as a first order approximation as:

$$L_e \approx 20\log (\tau/T) \quad \text{dB} \quad (\text{for } \tau > 3 \cdot T) \quad (21)$$

which is shown in Fig. 4 as the upper curve.

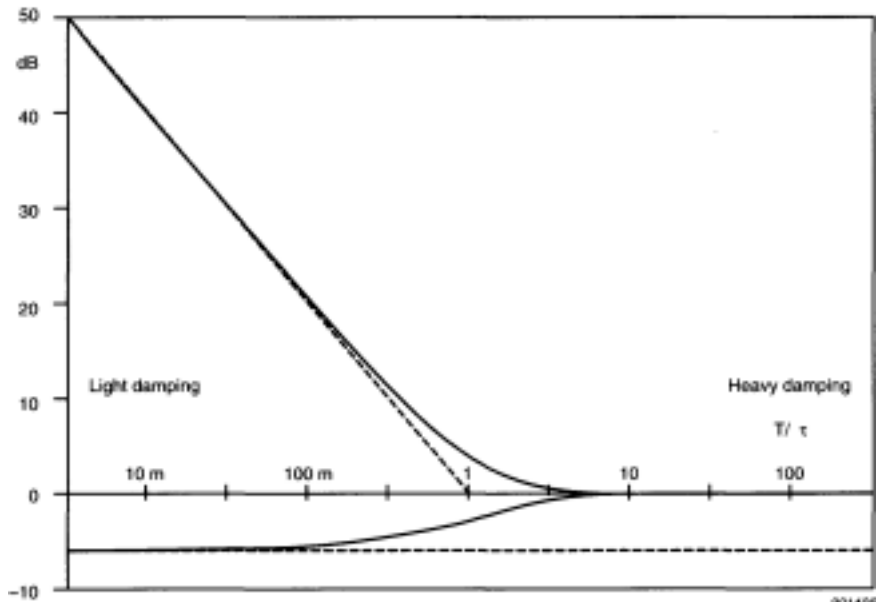


Fig. 4. Maximum amplitude error on Impulse Response Function as a function of relative damping

As seen, the amplitude error can be neglected if $T/\tau > 2.5$, in which case the impulse response is attenuated by approximately 20 dB at the end of the record. In the frequency domain this corresponds to a 3dB bandwidth of the system under test, which is larger than the DFT/FFT line spacing. As another example, if τ is 100 times longer than the record length, T , the amplitude error is 40dB.

Case 2: Resonance Exactly Between Two DFT Frequency Lines

In the case where the resonance is located exactly midway between line number k and $k+1$, equation (15) becomes

$$\omega_d = 2\pi \left(k + \frac{1}{2}\right) \cdot \Delta f \quad (22)$$

Thus equation (16) becomes

$$\omega_d i T = 2\pi \cdot i \cdot k + \pi \cdot i \quad (23)$$

For i even (0, -2, -4, etc.) we have

$$e^{j\omega_d i T} = e^{j\omega_d i T} = 1 \quad (24)$$

and for i odd (-1, -3, -5, etc.) we have

$$e^{j\omega_d i T} = e^{j\omega_d i T} = -1 \quad (25)$$

So in this case we have an amplitude error of

$$\epsilon_b = \sum_{i=0}^{\infty} e^{-i\sigma T} (-1)^i = \frac{1}{1 + e^{-T\sigma}} = \frac{1}{1 + e^{-T/\tau}} \quad (26)$$

As a first order approximation we have

$$\epsilon_b \approx \frac{1}{2} \quad (\text{for } \tau > 3 \cdot T) \quad (27)$$

Equation (27) shows that the amplitude is underestimated by a factor of 2 if the time constant of the system is considerably longer than the DFT/FFT record length.

On a dB (logarithmic) scale the error can be expressed as

$$L_e = -20 \log (1 + e^{-\sigma T}) \text{ dB} \quad (28)$$

and as a first order approximation

$$L_e = -20 \log (2) \text{ dB} = -6 \text{ dB} \text{ (for } \tau > 3 - T \text{)} \quad (29)$$

which is shown in Fig. 4 as the lower graph.

Time-Frequency Relationships

The amplitude error is seen to be given as a function of T/τ , i.e. the ratio between the record length (the analysis) and the time constant of the exponential decay (the damping descriptor). We could just as well use corresponding frequency domain descriptors, namely the line spacing Δf (the analysis) and the 3dB bandwidth Δf_{3dB} of the resonance peak (the damping descriptor).

The relationship between the different damping descriptors is shown in Table 1.

Natural frequency $\omega_0 = 2 \pi f_0$ ($\approx \omega_d$ for lightly damped resonances)					
Known	Unknown	$\Delta\omega =$	$\Delta f_{3dB} =$	$\zeta =$	$\sigma =$
3dB Bandwidth, $\Delta\omega$ (rad/s)	$\Delta\omega$	$\frac{\Delta\omega}{2\pi}$	$\frac{\Delta\omega}{2\omega_0}$	$\frac{\Delta\omega}{2}$	$\frac{2}{\Delta\omega}$
3dB Bandwidth, Δf_{3dB} (Hz)	$2\pi\Delta f_{3dB}$	Δf_{3dB}	$\frac{\Delta f_{3dB}}{2f_0}$	$\pi\Delta f_{3dB}$	$\frac{1}{\pi\Delta f_{3dB}}$
Fraction of critical damping, ζ ,	$2\zeta\omega_0$	$2\zeta f_0$	ζ	$2\pi f_0 \zeta$	$\frac{1}{2\pi f_0}$
Decay constant σ (s ⁻¹)	2σ	$\frac{\sigma}{\pi}$	$\frac{\sigma}{\omega_0}$	σ	$\frac{1}{\sigma}$
Time constant, τ (s)	$\frac{2}{\tau}$	$\frac{1}{\pi\tau}$	$\frac{1}{2\pi f_0 \tau}$	$\frac{1}{\tau}$	τ

Table 1. Interrelationship between different "damping" descriptors

The basic relationship between time and frequency domain descriptors of the damping for a SDOF model is

$$\tau \cdot \sigma = 1 \quad (30)$$

i.e. time constant multiplied by one half the 3dB bandwidth (in radians per second) equals unity. This relationship is sometimes called the uncertainty principle. If we increase the resolution in one domain, we lose resolution in the other, or if the event becomes narrower in one domain it becomes broader in the other.

Eq. (30) can also be rewritten as

$$\tau \cdot \Delta f_{3dB} = 1/\pi \quad (31)$$

If we combine Eq. (31) with the general time-frequency relationship for DFT/FFT analysis as indicated in Eq. (32),

$$T \cdot \Delta f = 1 \quad (32)$$

we get

$$\pi \cdot \frac{\Delta f_{3dB}}{\Delta f} = T \quad (33)$$

which shows that relative damping can be expressed both in the frequency and the time domain by easy to interpret numbers which only differ by a factor of π . Example: If the system 3dB bandwidth is equal to 10 times the line spacing, then the record length is 31.4 times longer than the system time constant.

General Case Error

The formula for the general case is shown in equation (13). Using the well-known relation

$$\sin(\alpha - \beta) = \sin \alpha \cdot \cos \beta - \cos \alpha \cdot \sin \beta \quad (34)$$

the impulse response can be written as

$$\begin{aligned}
\hat{h}(t) &= A_o e^{-\sigma t} \sum_{i=-\infty}^0 e^{i\sigma T} [\sin(\omega_d t) \cdot \cos(\omega_d iT) - \cos(\omega_d t) \cdot \sin(\omega_d iT)] \\
&= A_o e^{-\sigma t} \sin(\omega_d t) \sum_{i=-\infty}^0 e^{\sigma iT} \cos(\omega_d iT) \\
&\quad - A_o e^{-\sigma t} \cos(\omega_d t) \sum_{i=-\infty}^0 e^{\sigma iT} \sin(\omega_d iT)
\end{aligned} \tag{35}$$

which in a simplified form is

$$\hat{h}(t) = A_o e^{-\sigma t} \sin(\omega_d t) \cdot C_1 - A_o e^{-\sigma t} \cos(\omega_d t) \cdot C_2 \tag{36}$$

From eq. (36) it is clearly seen that the impulse response function can be expressed as a sum (difference) of two orthogonal exponentially decaying sinusoidal terms each weighted by a factor of C_1 and C_2 respectively, which are functions of σT and $\omega_d T$.

$$\begin{aligned}
C_1 &= \sum_{i=-\infty}^0 e^{\sigma iT} \cdot \cos(\omega_d iT) \\
&= \sum_{i=0}^{\infty} (e^{-\sigma T})^i \cdot \cos(\omega_d iT) \\
&= \frac{1 - e^{-\sigma T} \cdot \cos(\omega_d T)}{1 - 2e^{-\sigma T} \cdot \cos(\omega_d T) + e^{-2\sigma T}}
\end{aligned} \tag{37}$$

$$\begin{aligned}
C_2 &= \sum_{i=-\infty}^0 e^{\sigma i T} \cdot \sin(\omega_d i T) \\
&= - \sum_{i=0}^{\infty} (e^{-\sigma T})^i \cdot \sin(\omega_d i T) \\
&= \frac{e^{-\sigma T} \cdot \sin(\omega_d T)}{1 - 2e^{-\sigma T} \cos(\omega_d T) + e^{-2\sigma T}}
\end{aligned} \tag{38}$$

Thus the impulse response function can be expressed as the sum of two orthogonal terms 90° out of phase with each other. The IRF can also be represented by one term including a phase shift, as shown in eq. (39), which is merely a conversion of eq. (36) from rectangular to polar coordinates:

$$\hat{h}(t) = A_o e^{-\sigma t} \cdot C \cdot \sin(\omega_d t - \varphi) \tag{39}$$

where

$$C = \sqrt{C_1^2 + C_2^2} = \sqrt{(1 - 2e^{-\sigma T} \cos(\omega_d T) + e^{-2\sigma T})^{-1}} \tag{40}$$

is the amplitude error and

$$\varphi = \arctan(C_2/C_1) = \arctan \left[\frac{e^{-\sigma T} \sin(\omega_d T)}{1 - e^{-\sigma T} \cos(\omega_d T)} \right] \tag{41}$$

is the phase error.

In the general case the amplitude error is found to have values between the limits shown in Fig. 4. Eight different cases including the curves from Fig. 4 are shown in Fig. 5. Please note that the x-axis is scaled differently from Fig. 4

according to equation (33). Thus Fig. 4 shows the error as a function of relative damping using the time domain damping descriptor τ , while Fig. 5 shows the error as a function of relative damping using the frequency domain damping descriptor, $\Delta f_{3\text{dB}}$.

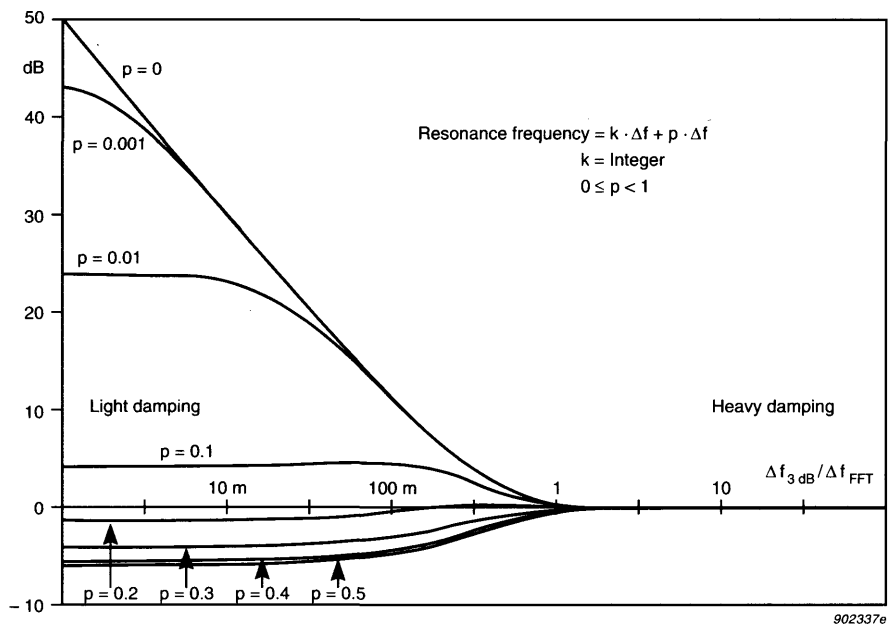


Fig. 5. Amplitude error of Impulse Response Function as a function of relative damping, for eight different cases of resonant frequencies

Fig. 6 shows the amplitude error as a function of resonance frequency in the interval between two DFT frequency lines. Four different damping cases are shown, namely where the system 3 dB bandwidth equals the line spacing and where the 3 dB bandwidth is 10, 100 and 1000 times narrower than the line spacing. It is clearly seen that overestimation only occurs when the natural frequency is in the vicinity of a DFT frequency line.

Fig. 7 shows the phase error as a function of frequency for the same four damping cases. There is no phase error in the two previous mentioned special

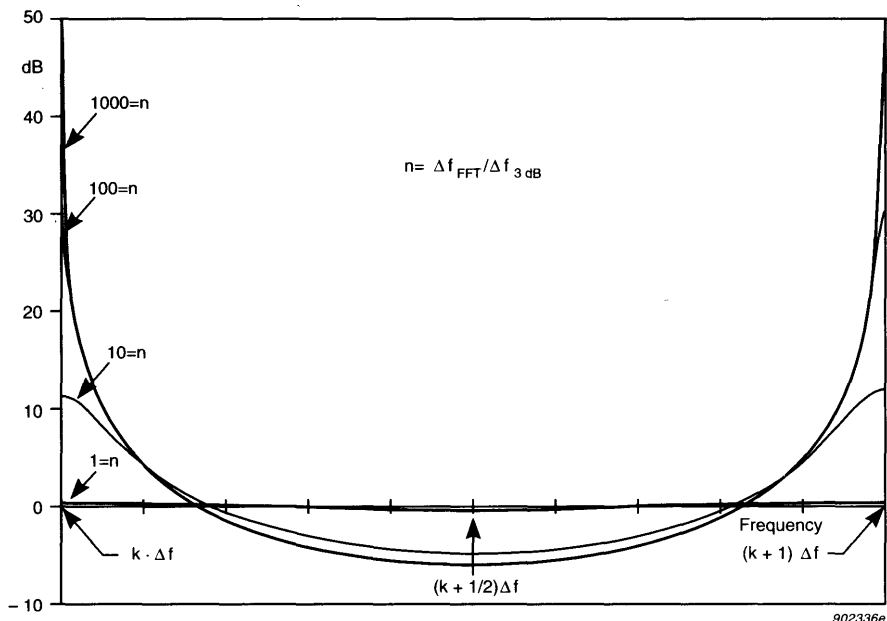


Fig. 6. Amplitude error of Impulse Response Function as a function of frequency, where k is DFT line no. k and $(k + 1)$ is DFT line no. $(k + 1)$. Four different damping cases are shown

cases, where the natural frequency either coincides with a spectral line or is exactly midway between two spectral lines. Furthermore, Figs. 6 and 7 show that the biggest amplitude and phase errors for very lightly damped system are found when the resonance frequency is close to a DFT spectral line.

As a final remark we can conclude that the errors can be neglected if the 3dB bandwidth of the system under test is broader than the DFT line spacing.

Computer Simulations

The theory and Figs. 4 to 7 have been verified by synthesizing FRFs with different damping and resonance frequencies. Both frequency domain and time domain curve fitters have been used to extract the system parameters (modal parameters). The modal software STAS SE v. 5.02 from ŠMS (Brüel&Kjær Type number WT 9100) has been used for these simulations.

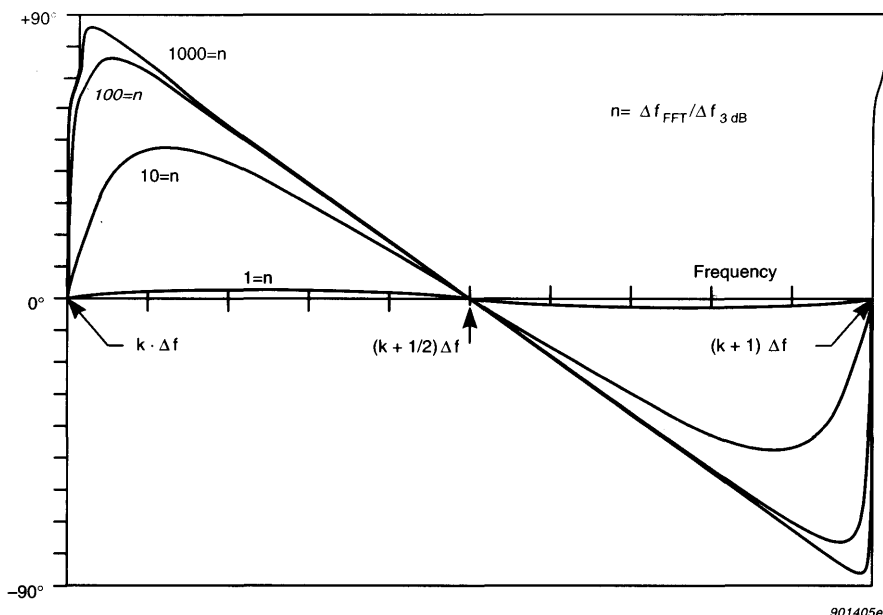


Fig. 7. Phase error on the Impulse Response Function as a function of frequency, where k is DFT line no. k and $(k + 1)$ is DFT line no. $(k + 1)$. Four different damping cases are shown

Measurement Conditions and Equipment Used

Some FRF measurements were performed on a freely suspended aluminium plate with the dimensions of 30cm x 25cm x 2cm. The structure was excited via a nylon stinger by a small Brüel & Kjær Vibration Exciter Type 4810 using a pseudo-random signal. The force signal was measured using a Brüel & Kjær Force Transducer Type 8200. The output vibration signal was measured using a small, lightweight (~2.4g) Brüel & Kjær Accelerometer Type 4375. The force and vibration signals were analysed using the Brüel & Kjær Multichannel Analysis System Type 3550 (DFT/FFT). A similar set-up is shown on the cover of this Technical Review.

Measurement Results

The modal parameters of the first resonance were determined using different resolutions, Δf , chosen in binary steps from 0.125 Hz to 16 Hz (see Table 2). The resonance of interest, located at 860.2 Hz, had a 3dB bandwidth of approximately 150 mHz corresponding to a time constant, τ of 2.1 s.

FFT Resolution		Relative Resolution		FRF Curve-fit			IRF Curve-fit		
Δf (Hz)	T (s)	$\Delta f_{3\text{dB}}/\Delta f$	T/ τ	ζ (m%)	R (dB)	$\angle R$ ($^{\circ}$)	ζ (m%)	R (dB)	$\angle R$ ($^{\circ}$)
0.125	8	1.24	3.9	10	82.5	179	10	82.2	183
0.25	4	0.62	1.9	9	82.4	180	9	81.4	175
0.5	2	0.31	0.97	9	82.5	180	8	81.0	197
1	1	0.15	0.49	9	82.4	179	9	83.9	218
2	0.5	77m	0.24	9	82.4	179	9	86.9	232
4	0.25	39m	0.12	10	82.4	179	10	92.4	238
8	0.125	19m	61m	9	82.4	179	9	76.7	175
16	62.5m	10m	30m	11	82.4	179	10	79.9	134

Table 2. Resolution, record length, number of spectral lines per 3dB bandwidth, number of time constants per record length, damping estimate as function of critical damping from an FRF curve-fit, estimate of residue both magnitude and phase, estimate of damping and residue from an IRF curve-fit. In all cases the damped natural frequency was estimated within 6m% standard deviation

Both time as well as frequency domain curve fitters have been applied to the measurements. It can be seen when dealing with light damping that the time domain curve fitter extracts correct damping and resonance frequency (pole location) but incorrect residues.

In Fig. 8, plots of the impulse response function are shown for four cases. The magnitude of the analytical (complex) impulse response function is displayed. The analytical impulse response function is obtained by use of the Hilbert transform. The Hilbert transform of the real valued impulse response function $h(t)$ (the real part) gives the imaginary part $j\sim h(t)$, and the analytical impulse response function is defined as

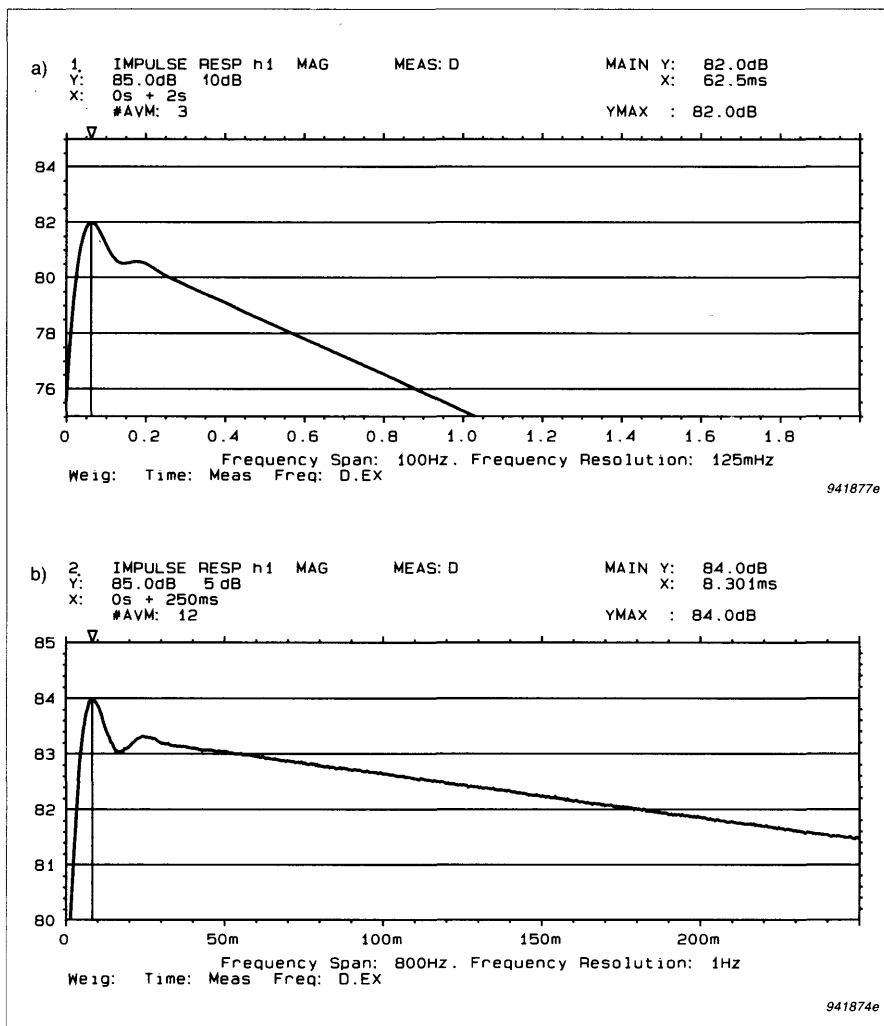


Fig. 8. Impulse response function for different resolutions, only the first half is shown. Note the difference in Y_{max} level near time zero for the four different cases
a) $\Delta f = 125 \text{ mHz}$, b) $\Delta f = 1\text{Hz}$,

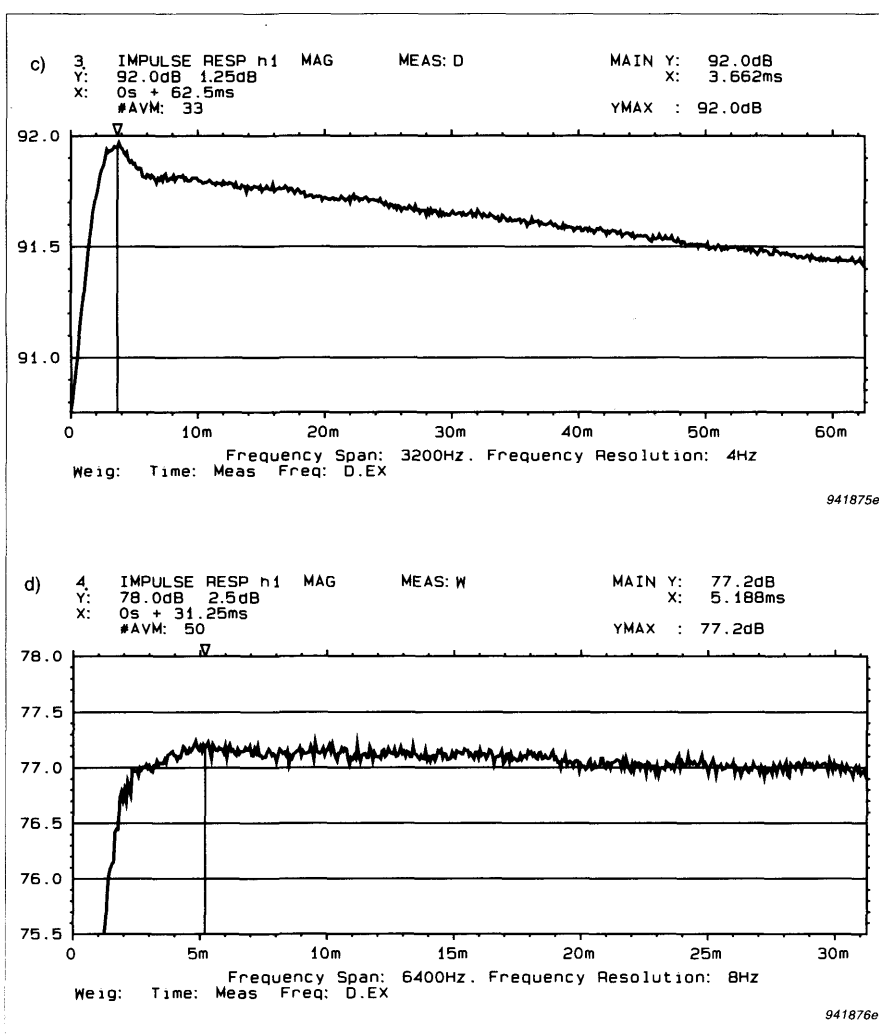


Fig.8 (cont.) Impulse response function for different resolutions, c) $\Delta f = 4$ Hz and resonance coinciding with a frequency line, d) $\Delta f = 8$ Hz and resonance exactly between two frequency lines

$$\hat{h}(t) = h(t) + j\tilde{h}(t) \quad (42)$$

The magnitude of the impulse response function is then given by

$$|\hat{h}(t)| = \sqrt{h^2(t) - \tilde{h}^2(t)} \quad (43)$$

The magnitude $|\hat{h}(t)|$ can be considered as being the envelope of $h(t)$. For the SDOF system (eq.(11)), the magnitude of the impulse response function becomes

$$|\hat{h}(t)| = A_0 e^{-\sigma t} \quad (44)$$

The advantages of using the magnitude instead of the real part are that the magnitude does not feature the oscillations (given by the term $\sin(\omega_d t)$) and that the magnitude can be shown on a logarithmic (dB) amplitude scale. A logarithmic amplitude scale gives more "dynamic" range in the presentation and reveals the exponential decay (given by the term $e^{-\sigma t}$) as a straight line.

The magnitude of the estimated impulse response function $\hat{h}(t)$ is $A_0 e^{-\sigma t} \cdot C$ (eq. (39)) which on a logarithmic (dB) scale becomes $-\sigma t \cdot 10 \log_e^2 + \text{constant} = -8.69t/\tau + \text{constant}$, i.e. a straight line with a slope of -8.69 dB per time constant τ . The magnitude at time $t=0$ is given by $A_0 C$. The damping value is thus estimated from the slope and the residue is estimated from the magnitude at time $t=0$, found by extrapolation of the straight line of the decay back to time $t=0$.

The four cases in Fig.8 represent situations where the line spacing Δf is:

- a) approximately equal to the 3 dB bandwidth of the resonance
- b) 6 times the 3 dB bandwidth
- c) 24 times the 3 dB bandwidth and the resonance frequency nearly coinciding with an analysis line
- d) 48 times the 3 dB bandwidth and the resonance frequency nearly midway between two analysis lines.

In all four cases a correct decay constant, i.e. damping value, was found and the natural frequency was correct as well. For the magnitude, extrapolated back to time $t=0$, giving the residue, we have correct results only in case a), a slight overestimation in case b), high overestimation (10dB) in case c) and a moderate underestimation (5dB) in case d).

As seen from Table 2, the phase error, as expected, is very high, 58 degrees (238 - 180) in case c). In case d) the phase error is only 5 degrees, which also confirms the theory.

The authors experienced difficulties for both time and frequency domain curve fitters when the 3dB bandwidth was more than 200 times narrower than the line spacing. The problem is that we have too few frequency samples of the resonance. In this case an exponential weighting function with the identical time or decay constant, σ_w , could be applied to both excitation and response signal. This will widen the measured bandwidth of the resonances. The residue and damped natural frequency will be correctly estimated, but the damping overestimated, as shown in Eq. (45):

$$\begin{aligned}\hat{h}(t) &= A_o e^{-\sigma t} \cdot e^{-\sigma_w t} \cdot C \cdot \sin(\omega_d t - \varphi) \\ &= A_o e^{-(\sigma + \sigma_w)t} \cdot C \cdot \sin(\omega_d t - \varphi) \\ &= A_o e^{-\sigma_m t} \cdot C \cdot \sin(\omega_d t - \varphi)\end{aligned}\quad (45)$$

Thus the exponential weighting function behaves as an "antialiasing" filter. This means that the correct damping can easily be calculated from the measured damping if the decay constant (the reciprocal of the time constant or length) of the exponential weighting is known:

$$\sigma = \sigma_m - \sigma_w \quad (46)$$

Applying the exponential weighting actually corresponds to not measuring the Transfer Function, $H(s)$, along the $j\omega$ axis, $H(j\omega)$, but along a line parallel to the $j\omega$ -axis crossing the real axis (σ or damping axis) at σ_w in the right half plane. Thus the residue and the damped natural frequency will be correctly estimated.

Conclusion and Final Remarks

It has been shown that the impulse response function, when calculated from the frequency response function using DFT/FFT techniques, in some practical applications suffers a bias error. The bias error is caused by an aliasing effect

which appears during the inverse DFT/FFT from the frequency domain (FRF) to the time domain (IRF).

The error becomes significant when leakage free measurements of lightly damped systems are performed and the resolution in the analysis is not sufficiently high compared to the bandwidth of the resonance peaks. The error can be neglected if the 3dB bandwidth of the resonances is greater than the line spacing Δf .

The SDOF system with viscous damping has been investigated (eq.(39)). The error can in this case be expressed by an amplitude error (eq. (40)) and a phase error (eq. (41)). Both of these are given by the ratio of the record length T to the time constant τ (or the ratio of the 3dB bandwidth Δf_{3dB} to the line spacing Δf) and the location of the damped natural frequency ω_d relative to the location of the frequency lines in the analysis.

The exponential decay, determined by the damping in the system, is not affected in the case of viscous damping. For other types of damping mechanisms, however, the aliasing effect could influence the damping value estimation.

When the impulse response function is used for mathematical modelling, such as in modal analysis, the error is directly reflected in the residues of the resonances and the given corrections have to be applied.

Special care should be taken when modal analysis is performed using single input/single output measurements with a shaker and one accelerometer. The accelerometer is in this case moved to a different position for each measurement. This can cause the damped natural frequency to be different in the different measurements due to the mass loading effect. The bias error will therefore be different for each individual measurement and, if the corrections are not applied on the estimated residues, the resulting mode shapes will be contaminated with what appears to be a random error.

Leakage free measurements can be obtained by using a proper excitation signal, such as pseudo-random, multisine, periodic random or burst random and applying rectangular weighting in the analysis.

If a random signal is used for excitation and Hanning weighting is applied in the analysis, at least 10 FFT lines per 3dB bandwidth are required to make the measurement appear leakage free [2, 3], and no effect of the bias error will be observed in the impulse response function. If the measurement is not performed with the required resolution, leakage will smear out the resonance peaks causing a so-called resolution bias error [1]. The resulting error in the estimated impulse response function can in this case not be compensated for.

For impulse excitation (hammer or impact excitation in structural analysis) an exponential weighting must be applied to the response signal to force this signal to be attenuated by approximately 40 dB at the end of the record. In this situation there will only be an influence of the exponential weighting which will appear as well-defined leakage. This can be compensated for as indicated in eq. (46) (see also [3]) and no effect of the aliasing is observed on the impulse response function.

References

- [1] H. HERLUFSEN: *Dual Channel FFT Analysis (Parts I & II)*, Brüel & Kjær Technical Review Nos. 1 & 2, 1984
- [2] S. GADE & H. HERLUFSEN: *Use of Weighting Functions in DFT/FFT Analysis*, Brüel & Kjær Technical Review Nos. 3 & 4, 1987
- [3] S. GADE & H. HERLUFSEN: *Digital Filter Techniques vs. FFT Techniques for Damping Measurements*, Brüel & Kjær Technical Review No. 1, 1994

Complex Modulus and Damping Measurements using Resonant and Non-resonant Methods

by S. Gade, K. Zaveri, H. Konstantin-Hansen and H. Herlufsen

Abstract

Traditional methods of damping measurement involved the use of sinusoidal signals for the excitation at low frequencies for bending resonances of specimens and at high frequencies for longitudinal resonances. With the advent of the dual channel real-time analyzers, wide-band random excitation can be conveniently used to excite and measure the response of the specimens simultaneously, whereby considerable time savings can be achieved. Two methods, one non-resonant and the other resonant, are outlined, the former yielding the real and elastic modulus as a continuous function of frequency. The results of the two methods are also compared.

Resume

Les anciennes mesures d'amortissement faisaient intervenir des signaux d'excitation sinusoïdaux, à basse fréquence pour les résonances de flexion, et à haute fréquence pour les résonances longitudinales. Les analyseurs bicanaux temps réel autorisent aujourd'hui un considérable gain de temps en permettant l'utilisation de signaux aléatoires large bande pour l'excitation et la mesure de la réponse simultanées de l'objet testé. Deux méthodes sont ici comparées, ainsi que leurs résultats respectifs, l'une faisant intervenir le phénomène de résonance, l'autre non. Cette dernière méthode donne le module d'élasticité et le module réel comme une fonction de réponse en fréquence continue.

Zusammenfassung

Traditionelle Methoden für Dämpfungsmessungen pflegten sinusförmige Signale zur Anregung zu verwenden: tiefe Frequenzen für Biegsresonanzen von Prüflingen und hohe Frequenzen für longitudinale Resonanzen. Mit Breitband-Rauschanregung durch Zweikanal-Echtzeitanalysatoren ist es

möglich geworden, auf bequeme Weise die Prüfstruktur gleichzeitig anzuregen und ihr Antwortverhalten zu messen, was eine beträchtliche Zeiter spart bedeutet. Zwei Methoden, eine nichtresonante und eine resonante, werden skizziert, von denen die erstgenannte den reellen und Elastizitätsmodul als kontinuierliche Funktion der Frequenz liefert. Es erfolgt ein Vergleich der Ergebnisse beider Methoden.

Nomenclature

<i>a</i>	acceleration [m/s ²]
<i>c</i>	viscous damping coefficient [N · s/m]
<i>d</i>	deflection [m]
<i>e</i>	base of natural logarithm, 2.72...
<i>f</i>	force [N]
<i>f_o</i>	undamped natural frequency [Hz]
<i>j</i>	imaginary number, $\sqrt{-1}$
<i>k</i>	kilo, 10 ³
<i>k</i>	stiffness [N/m]
<i>l</i>	length of isolator [m]
<i>m</i>	mass [kg]
<i>t</i>	time [s]
<i>v</i>	velocity [m/s]
<i>x</i>	displacement [m]
<i>ẋ</i>	velocity [m/s]
<i>ẍ</i>	acceleration [m/s ²]
<i>A</i>	cross sectional area of isolator [m ²]
<i>E*</i>	complex elastic modulus [N/m ²]
<i>E'</i>	modulus of elasticity. Young's modulus [N/m ²]
<i>E''</i>	loss modulus [N/m ²]
<i>F</i>	force spectrum [N · s]
<i>H</i>	compliance frequency response function [m/N]
<i>X</i>	displacement spectrum [m · s]
ε	sinusoidal strain [dimensionless]
$\hat{\varepsilon}$	strain, (relative elongation, Δ/l) [dimensionless]
η	loss factor [dimensionless]
π	pi, 3.14...
θ	angle of complex modulus [rad]
σ	sinusoidal stress [N/m ²]
$\hat{\sigma}$	stress [N/m ²]

ω	angular frequency [rad/s]
ω_o	undamped natural frequency [rad/s]
Δf	3 dB bandwidth [Hz]
Δl	elongation of isolator [m]

Introduction

The stress-strain relationship of visco-elastic materials, generally used in the damping treatment of structures, can be described by two properties, such as the perfectly elastic (in-phase) stress-strain modulus and the loss factor. The values of these properties need to be determined in tension or compression for materials used as unconstrained damping layers and as anti-vibration mountings under machinery and under foundation blocks.

Using a dual channel FFT analyzer, the specimen can be excited using wide-band random excitation, and the properties determined from the frequency response spectra, as a continuous function of frequency, as shown in the following.

Another possibility is to preload the specimen by a well-known mass, such that the preloaded damping material becomes a part of a resonant mass-spring-damper system. Damping, e.g. loss factor, is then determined from the 3 dB bandwidth of the resonance. The procedure is then repeated at different frequencies of the specimen using different mass-loadings.

The two methods are demonstrated and compared in this article.

Theory for the Non-resonant Method

As most elastomers are elastically imperfect, the strain lags the stress. An applied sinusoidal stress (force per area) usually results in a sinusoidal strain (relative elongation $\Delta l/l$), the phase angle θ between them remaining constant during a complete strain cycle, although it can vary with the strain amplitude and the frequency.

Let σ be a sinusoidal stress applied which, using complex notation, can be written as:

$$\sigma = \sigma \times e^{j\omega t} \quad (1)$$

The strain, e , resulting from this stress will be:

$$\varepsilon = \varepsilon \times e^{j(\omega t - \theta)} \quad (2)$$

Thus the complex elastic modulus, E^* , is:

$$E^* = \frac{\sigma}{\varepsilon} = \frac{\hat{\sigma}}{\hat{\varepsilon}} \times e^{j\theta} \quad (3)$$

The coincident (in phase) elastic modulus (modulus of elasticity or Young's Modulus), E' , will be given by:

$$E'' = \left(\frac{\hat{\sigma}}{\hat{\varepsilon}} \right) \times \cos \theta \quad (4)$$

and the quadrature (90° out of phase) loss modulus, E'' , will be given by:

$$E'' = \left(\frac{\hat{\sigma}}{\hat{\varepsilon}} \right) \times \sin \theta \quad (5)$$

The amount of imperfect elasticity possessed by the material is given by the ratio of these two moduli and is denoted by the loss factor η as:

$$\eta = \frac{E''}{E'} = \tan \theta \quad (6)$$

Fig. 1 shows a vector diagram illustrating these quantities, where E^* represents the complex modulus. Thus only two properties need to be measured, either E^* and θ or E' and E'' (Magnitude/Phase or Real/Imaginary parts).

As stress is force F divided by area A and strain is deflection divided by original length l , eqs. (4) and (5) may be written as:

$$E' = \frac{|F|}{|d|} \times \frac{l}{A} \cos \theta = \text{Real} \frac{(F)}{(d)} \times \frac{l}{A} \quad (7)$$

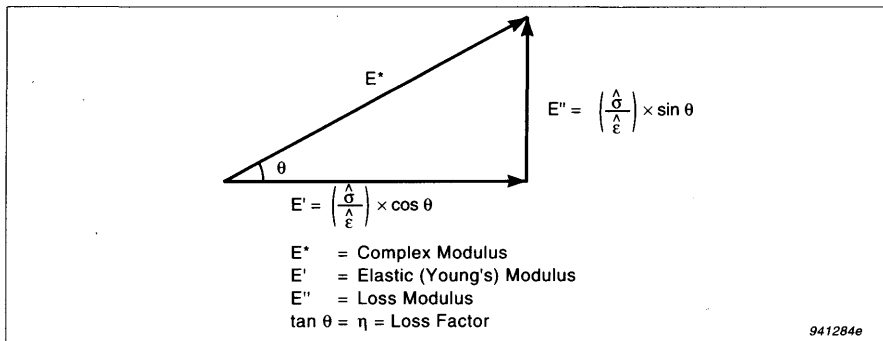


Fig. 1. Vector presentation of various moduli

$$E'' = \frac{|F|}{|d|} \times \frac{l}{A} \sin \theta = \text{Imaginary} \left(\frac{F}{d} \right) \times \frac{l}{A} \quad (8)$$

where A is the cross-sectional area of the isolator and l is the length of the isolator.

For random excitation, the ratio offeree to displacement, the dynamic stiffness, can be determined as the frequency response function between the force and displacement (acceleration integrated twice). The theory behind frequency response function measurements is found in Ref. [1].

The dynamic stiffness, being complex, can either be measured as magnitude and phase or as real and imaginary parts. By multiplying the dynamic stiffness by the length of the isolator and dividing by the cross-sectional area of the isolator, we obtain the complex elastic modulus E^* . The loss factor is given by the phase measurement.

A rigorous derivation of the theory can be found in Ref. [2].

Theory for the Resonant Method

By mounting a mass on top of the visco-elastic material, the combination behaves as a simple mass-spring-dashpot system, i.e., a single degree of freedom (SDOF) system, Fig.2.

Using Newton's second law and time domain formulation, we obtain:

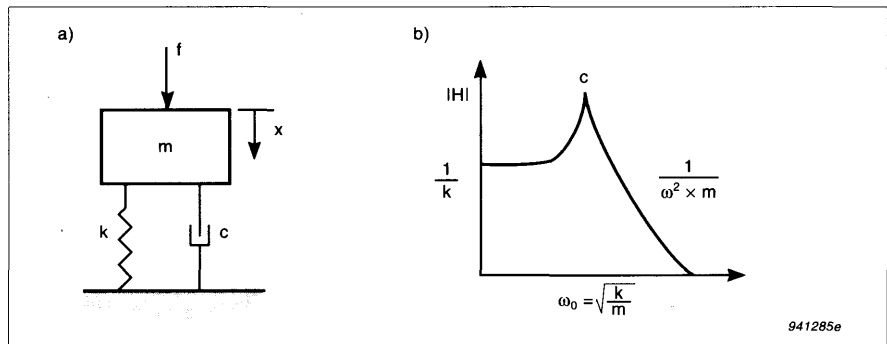


Fig. 2. a) A SDOF, Single Degree of Freedom Model, b) The magnitude of the frequency response functions $|H|$ of a SDOF model

$$\begin{aligned} f(t) &= m \times a(t) + c \times v(t) + k \times x(t) \\ &= m \times \ddot{x}(t) + c \times \dot{x}(t) + k \times x(t) \end{aligned} \quad (9)$$

Using the fact that differentiation corresponds to multiplication by $j\omega$ in the frequency domain, we obtain the following expression for the compliance Frequency Response Function, FRF:

$$H(\omega) = \frac{X(\omega)}{F(\omega)} = \frac{1}{-m\omega^2 + jc\omega + k} = \frac{1}{(k - m\omega^2) + jc\omega} \quad (10)$$

which shows that the compliance FRF equals the reciprocal of the stiffness, k , at low frequencies and that the accelerance FRF equals the reciprocal of the applied mass at high frequencies. See Fig. 2.

At the resonance frequency, ω_0 the real part of eq.(10) becomes zero and the level is exclusively determined by the damping mechanism, c .

The resonance frequency is given by the square root of the ratio between stiffness and mass:

$$\omega_0 = 2\pi f_0 = \sqrt{\frac{k}{m}} \quad (11)$$

It can be shown that the loss factor, η , a measure for the damping, is given by the ratio between the 3 dB bandwidth, Δf , and the resonance frequency, f_o :

$$\eta = \frac{\Delta f}{f_o} \quad (12)$$

Different mass loadings yield damping at different frequencies. For random excitation the ratio of displacement to force (mobility type of calculation), the dynamic compliance, can be determined as the frequency response function between displacement (acceleration integrated twice) and force.

More detailed information about damping measurements using resonant methods is found in Ref.[3].

Experimental Procedure and Results for the Non-resonant Method

Fig.3 shows the instrumentation set-up used for the determination of the complex modulus and the loss factor of elastomers used for anti-vibration mountings. One isolator (machine-shoe) was placed on a seismic mass (concrete floor) and excited by a shaker via a nylon stinger. The excitation force was

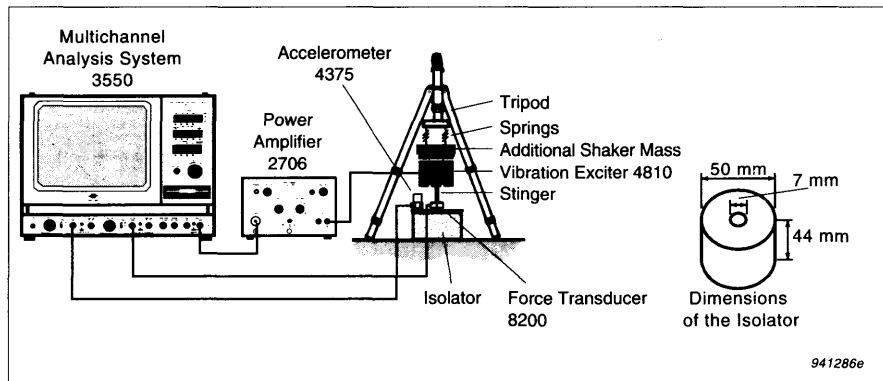


Fig. 3. Instrumentation set-up and dimensions of isolator

measured using a force transducer. An accelerometer was mounted beside the force transducer such that the force and the acceleration input to the isolator could be measured directly. The acceleration and force signals were fed to channels A and B of the analyzer, respectively. The shaker was fed a random noise signal from the generator section of the analyzer. The force and acceleration signals were both Hanning weighted, and the acceleration signal double integrated in the analyzer for determining the displacement. See Fig.3.

Fig. 4 (lower) shows the measurement set-up giving the parameters chosen on the analyzer, while Fig.4 (upper) shows the magnitude of the stiffness Frequency Response Function. The cursor reading indicates a static stiffness of approximately $k = 130$ kN/m. The coherence function was unity at all frequencies (except below 10 Hz), illustrating a linear dependency between force and displacement signals. See also Fig. 11.

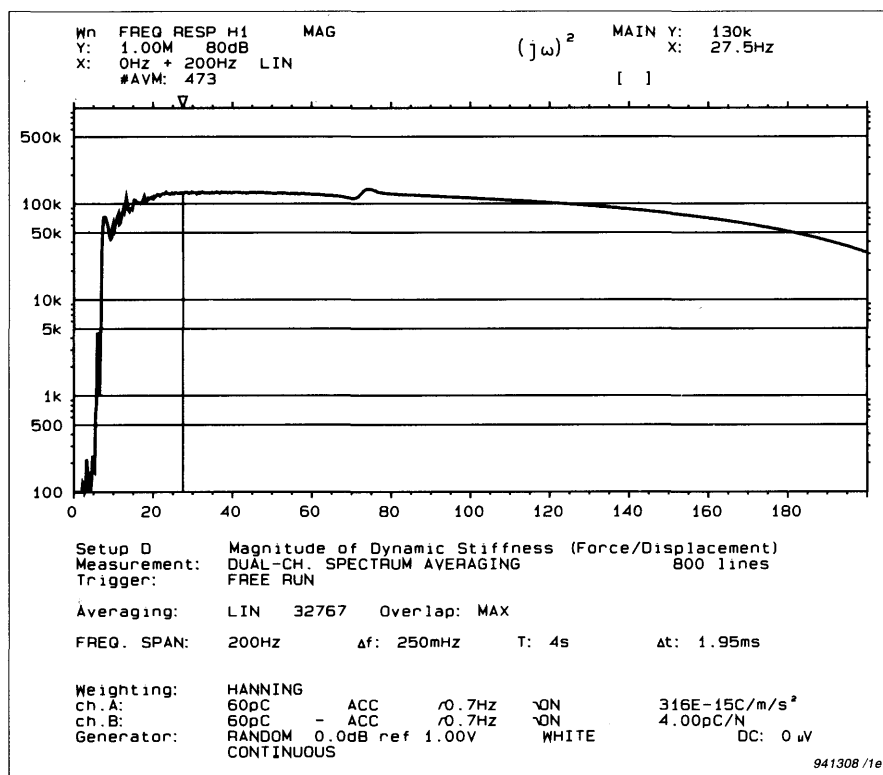


Fig. 4. The magnitude of the dynamic stiffness Frequency Response Function and Measurement set-up

Fig. 5 (upper and lower) shows the autospectra of the displacement and force signals respectively. The shapes of both these curves are similar, illustrating the spring-like behaviour of the isolator.

Fig. 6 shows the magnitude of the Complex Modulus, E^* . Thus the dynamic stiffness has been rescaled in the transducer set-up by a factor of $l/A = 22.41\text{m}^{-1}$, which is the ratio between the length, l and the cross-sectional area, A , of the isolator. (0.9941 is the transducer sensitivity "adjust".) The irregularity found at 75Hz is due to a stinger resonance. This was confirmed by using a stinger with different dimensions.

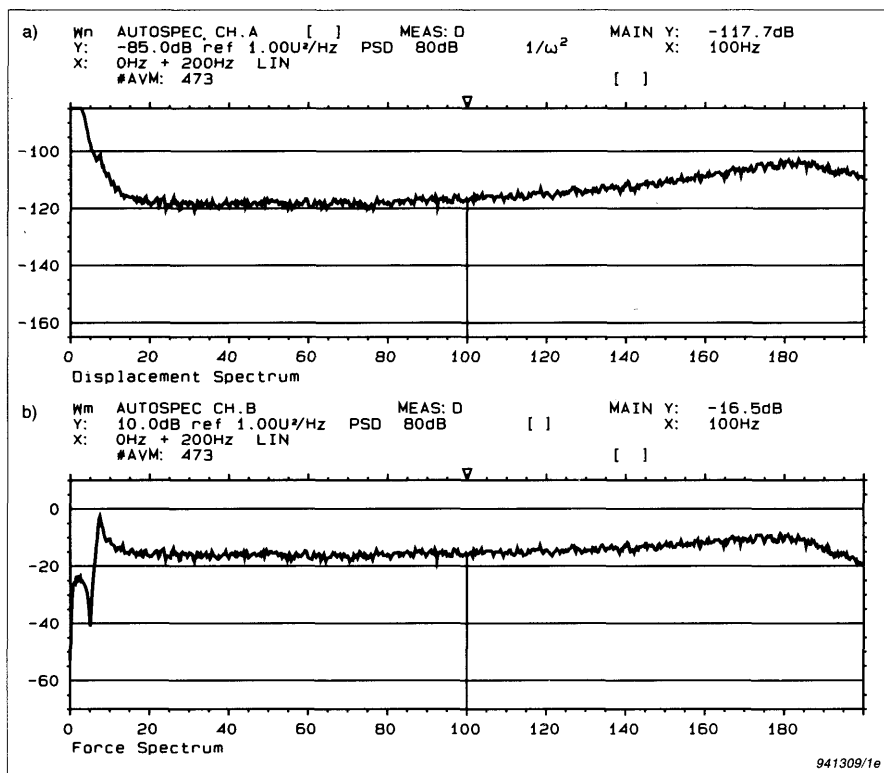


Fig. 5. Autospectra of displacement and force signals

Instead of plotting the magnitude and phase, the real and the imaginary parts of the dynamic complex modulus, i.e. the elastic (Young's) modulus and loss modulus can also be plotted as shown in Fig. 7 a) and b), respectively. It can be seen that for increasing frequency, the elastic modulus has a decreasing tendency whereas the loss modulus (i.e. the damping characteristics) seems to increase.

The loss factor, η (i.e. damping), can now be calculated as a continuous function of frequency simply by taking the tangent to the phase, $\tan(\theta)$. This is implemented in the analyzer as a simple User Definable Display Function and shown in Fig. 8b).

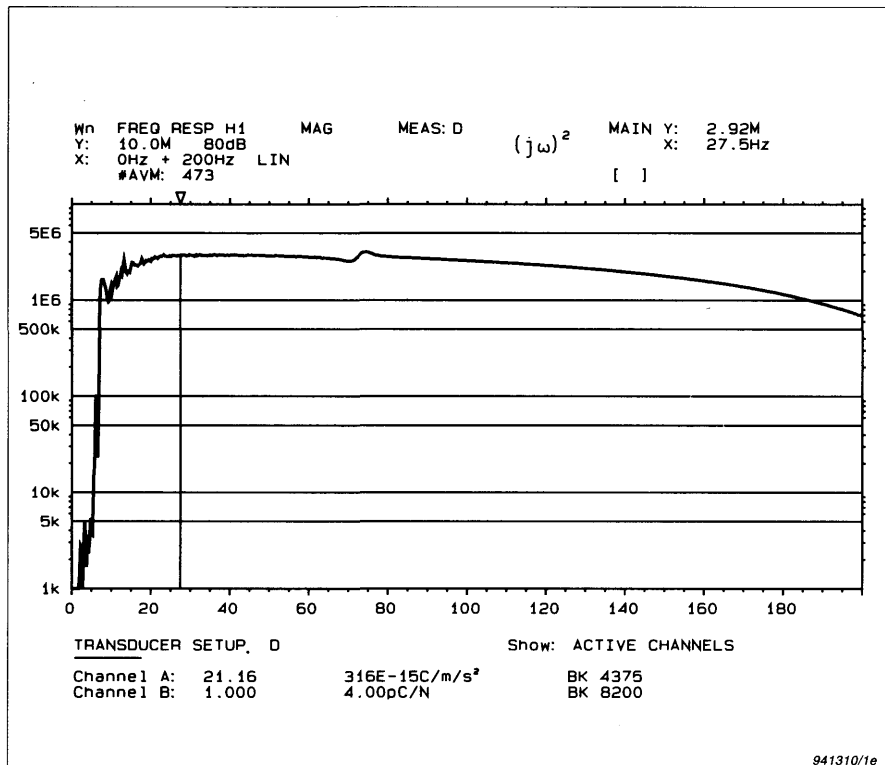


Fig. 6. Magnitude of Complex Modulus. Rescaling is done in the transducer set-up: $0.9941 \times 22.41 = 21.16$

The loss factor at 41 Hz is shown to be $\tan(4.5^\circ) = 0.076$ using the cursor readings. Some smoothing has been applied to the graph of the loss factor.

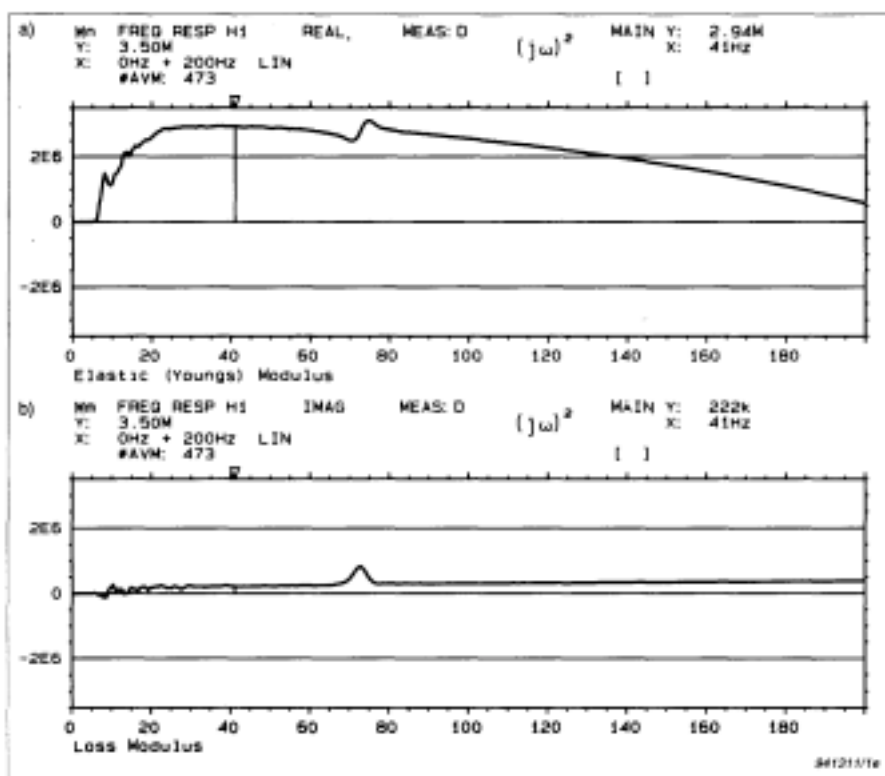


Fig. 7. a) Real part of complex modulus i.e. the elastic (Young's) modulus b) Imaginary part of complex modulus, i.e. the loss modulus

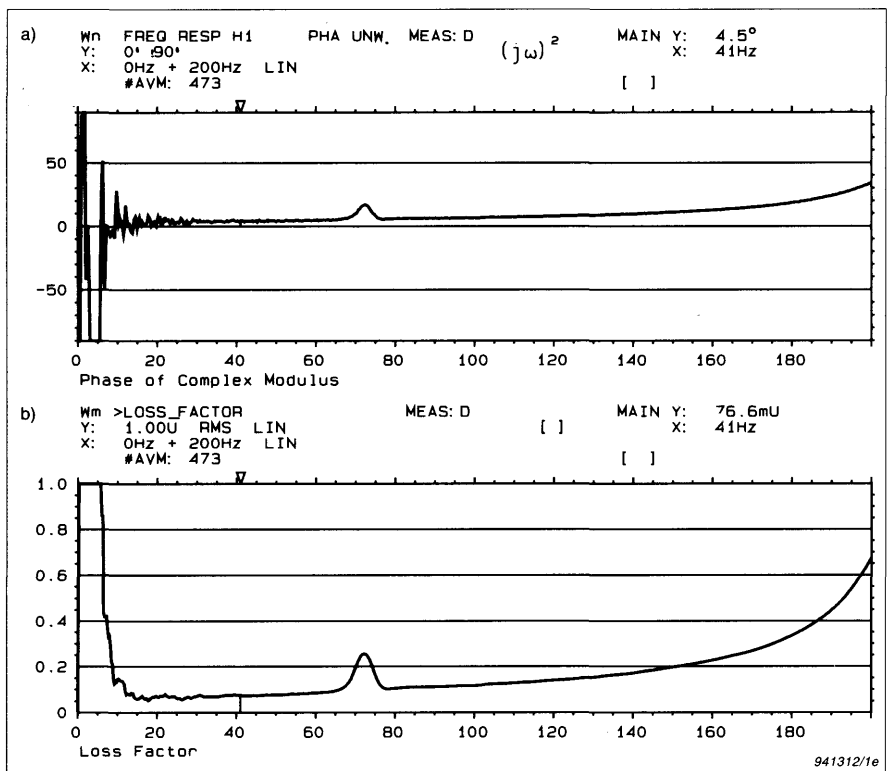


Fig. 8. a) Phase, θ of complex modulus b) Loss factor, η calculated as $\tan(\theta)$ via a User Definable Display Function

Experimental Procedure and Results for the Resonant Method

The set-up is similar to the one shown in Fig.3 except that a rigid mass (a block of steel) of 2kg was placed on top of the isolator. See Fig.9.

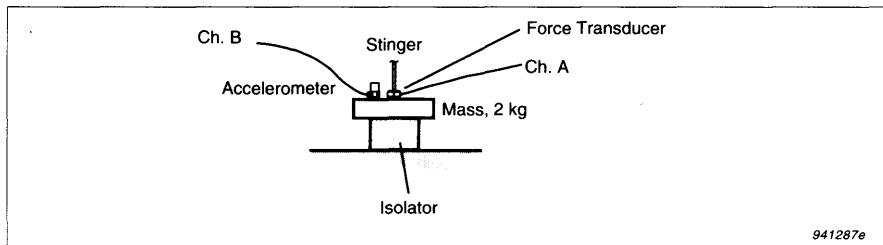


Fig. 9. A rigid mass of 2kg is mounted on top of the isolator

For convenience, the force transducer was connected to channel A and the accelerometer to channel B, in order to display mobility types of Frequency Response Functions directly, although the analyzer also includes the reciprocal of the measured frequency response function as a standard display function. Multisine excitation signal and rectangular weighting have been used in this case.

The result of this measurement is shown in Fig. 10 a). A resonance frequency is located at 42 Hz. A simple User Definable Auxiliary Information finds the 3dB bandwidth, $\Delta f = 3.25$ Hz, and thus the loss factor, $\eta = 3.25/42 = 0.076$, which is in agreement with the results obtained by the non-resonant method.

The static stiffness can be calculated from eq. (11): $k = (2\pi \times 42.625 \text{ Hz})^2 \times 2 \text{ kg} = 143\,000 \text{ N/m}$ which is within 10% of the results obtained with the non-resonant method.

Of course the static stiffness can be calculated by displaying the dynamic stiffness function, which is shown in the lower trace of Fig. 10b). The reciprocal of the acceleration function is multiplied by $(j\omega)^2$ in order to obtain the dynamic stiffness and cursor readings at lowest reliable frequency indicate a static stiffness of approximately 131kN/m.

In order to find damping at other frequencies, different mass loadings must be applied. In our case, measurement was repeated once with a 1kg mass.

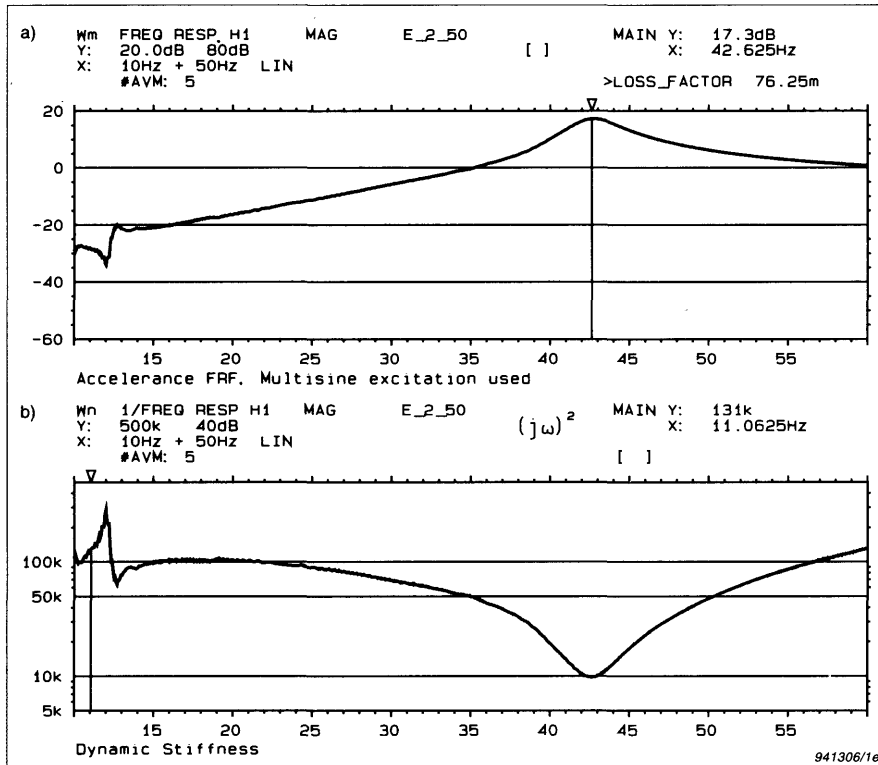


Fig. 10. a) Accelerance Frequency Response Function. Cursor readings indicate resonance frequency and loss factor, b) Dynamic Stiffness. Cursor reading indicates a static stiffness of approximately 131 kN/m

Examples of the results are shown in Fig. 11 a), which displays the dynamic stiffness. The resonance was located at 58.7 Hz ($\sim 42.6 \text{ Hz} \times \sqrt{2\text{kg}/1\text{kg}} = 60.2\text{Hz}$).

The 3 dB bandwidth was 4.4 Hz yielding a loss factor of 0.075 and a static stiffness of $k = 131\text{kN/m}$. The lowest reliable frequency is found by viewing the coherence function, which is shown in the lower trace of Fig. 11 b). Again the results from the non-resonant methods were confirmed.

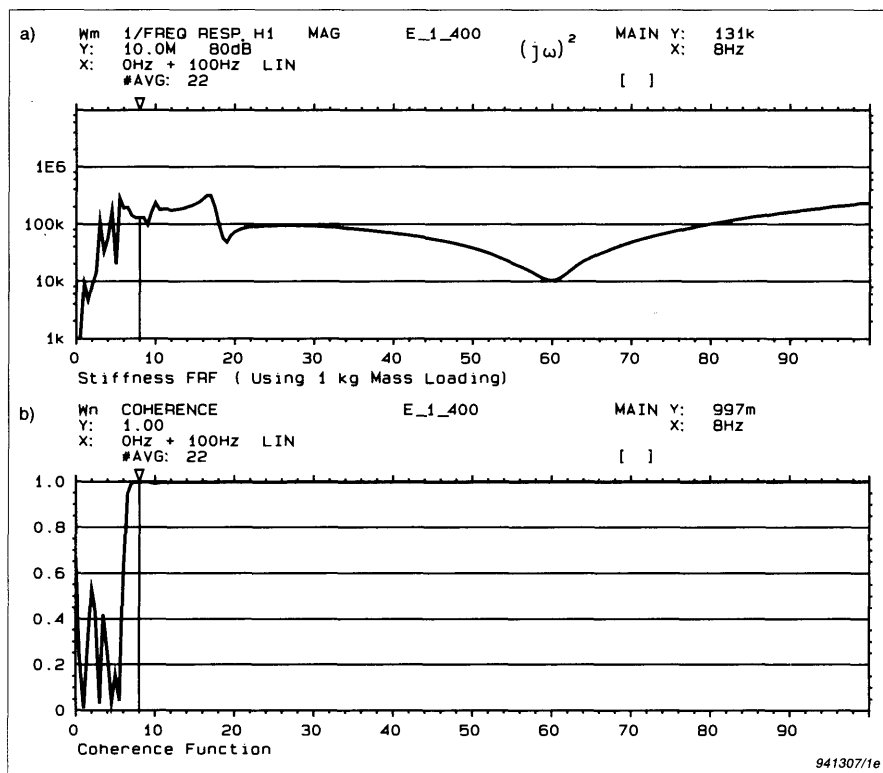


Fig. 11. a) Stiffness Frequency Response Function. Resonance found at 58.7 Hz. Cursor reading at 8 Hz indicates stiffness of 131 k.N/m. b) Coherence, lowest reliable frequency is found to be around 8 Hz

Conclusions

A relatively quick and easy method is described, whereby the elastic (Young's) and loss moduli as well as the loss factor of isolators and damping material can be obtained as continuous functions of frequency.

The results were verified at two frequencies using the well-known resonant method, where damping is calculated from a 3 dB bandwidth determination.

References

- [1] HERLUFSEN, H.: "*Dual Channel FFT Analysis (Part I & II)*", Brüel & Kjær Technical Review No. 1 & 2, 1984
- [2] GANERIWALA, S.N.: "*Characterization of Dynamic Viscoelastic Properties of Elastomers using Digital Spectral Analysis*", Ph.D. Thesis. University of Texas at Austin 1982.
- [3] GADE, S. & HERLUFSEN, H.: "*Digital Filter Techniques vs. FFT Techniques for Damping Measurements*", Brüel & Kjær Technical Review No. 1, 1994

Previously issued numbers of Brüel & Kjær Technical Review

(Continued from cover page 2)

2-1985 Heat Stress

A New Thermal Anemometer Probe for Indoor Air Velocity Measurements

1 -1985 Local Thermal Discomfort

4 -1984 Methods for the Calculation of Contrast

Proper Use of Weighting Functions for Impact Testing

Computer Data Acquisition from Brüel & Kjær Digital Frequency Analyzers 2131/2134 Using their Memory as a Buffer

3 -1984 The Hilbert Transform

Microphone System for Extremely Low Sound Levels

Averaging Times of Level Recorder 2317

2 -1984 Dual Channel FFT Analysis (Part II)

1 -1984 Dual Channel FFT Analysis (Part I)

4 -1983 Sound Level Meters - The Atlantic Divide

Design Principles for Integrating Sound Level Meters

3 -1983 Fourier Analysis of Surface Roughness

2 -1983 System Analysis and Time Delay Spectrometry (Part II)

1 -1983 System Analysis and Time Delay Spectrometry (Part I)

4 -1982 Sound Intensity (Part II Instrumentation and Applications)

Flutter Compensation of Tape Recorded Signals for Narrow Band Analysis

3 -1982 Sound Intensity (Part I Theory)

2 -1982 Thermal Comfort

Special technical literature

Brüel & Kjær publishes a variety of technical literature which can be obtained from your local Brüel & Kjær representative.

The following literature is presently available:

- Modal Analysis of Large Structures-Multiple Exciter Systems (English)
- Acoustic Noise Measurements (English), 5th. Edition
- Noise Control (English, French)
- Frequency Analysis (English), 3rd. Edition
- Catalogues (several languages)
- Product Data Sheets (English, German, French, Russian)

Furthermore, back copies of the Technical Review can be supplied as shown in the list above. Older issues may be obtained provided they are still in stock.

Brüel & Kjær



WORLD HEADQUARTERS: DK-2850 Nærum · Denmark

Telephone: +45 42 80 05 00 · Telex: 37316 bruka dk · Fax: +45 42 80 14 05

Australia (02) 450-2066 · Austria 00 43-1-816 74 00 · Belgium 016/44 9225 · Brazil (011) 246-8166

Canada: East (514) 695-8225 West (604) 591-9300 · China 1-84 19 625 · Czech Republic 02-67 02 1100

Finland (0)1481577 · France (1) 64 57 20 10 · Germany 06151/8149-0 · Great Britain (081) 954-2366

Holland 03402-39994 · Hong Kong 548 7486 · Hungary (1) 215 83 05/215 89 29 · Italy (02) 57 60 4141

Japan 03-5420-7302 · Republic of Korea (02) 554-0605 · Norway 66 90 4410 · Poland (0-22) 40 93 92

Portugal (1) 38 59 256/38 59 280 · Singapore 735 8933 · Slovak Republic 07-55666 · Spain (91) 368 10 00

Sweden (08) 71127 30 · Switzerland 01/940 09 09 · Taiwan (02) 713 9303 · Tunisia (01) 750 400 · USA (404) 981-9311

Local representatives and service organisations worldwide